IOP Publishing European Journal of Physics
Eur. J. Phys. 38 (2017) 023001 (13pp) doi:10.1088/1361-6404/aa5395

Review

Teaching hands-on geophysics: examples from the Rū seismic network in New Zealand

Kasper van Wijk[1], Jonathan Simpson and Ludmila Adam

University of Auckland, New Zealand

E-mail: k.vanwijk@auckland.ac.nz

Received 19 August 2015, revised 23 November 2016
Accepted for publication 13 December 2016
Published 16 January 2017

Abstract

Education in physics and geosciences can be effectively illustrated by the analysis of earthquakes and the subsequent propagation of seismic waves in the Earth. Educational seismology has matured to a level where both the hard- and software are robust and user friendly. This has resulted in successful implementation of educational networks around the world. Seismic data recorded by students are of such quality that these can be used in classic earthquake location exercises, for example. But even ocean waves weakly coupled into the Earth's crust can now be recorded on educational seismometers. These signals are not just noise, but form the basis of more recent developments in seismology, such as seismic interferometry, where seismic waves generated by ocean waves—instead of earthquakes—can be used to infer information about the Earth's interior. Here, we introduce an earthquake location exercise and an analysis of ambient seismic noise, and present examples. Data are provided, and all needed software is freely available.

Keywords: seismology, physics education, data processing

(Some figures may appear in colour only in the online journal)

1. Introduction

In a way, earthquakes are the exclamation mark to the dynamics of our planet. The sudden release of stress, built up by tectonic or volcanic processes, often has dramatic consequences. Earthquake signals can now easily be measured in classrooms around the world. Sensor development has accelerated with the advent of seismology after the 1906 earthquake of San

[1] Author to whom any correspondence should be addressed.

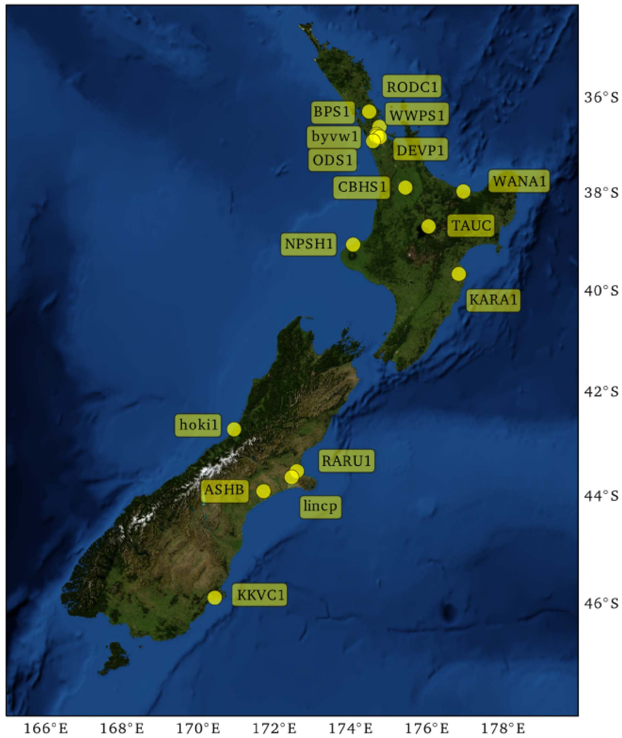

Figure 1. Station locations in the Rū network of educational seismometers in New Zealand. Map made with the free software Cartopy (Met Office 2010–2015). Made with Natural Earth. Free vector and raster map data @ www.naturalearthdata.com. Cartopy is published under the LGPLv3 licence.

Francisco. The Wood–Anderson seismograph was developed (Anderson and Wood 1925), as was a scale to describe the magnitude of earthquakes (Richter 1935). However, it was not until the publication of Lehman's design of a horizontal pendulum seismograph in Scientific American (Walker 1979), that a more general audience was able to record and analyse their own seismic data. The focus of the Lehman design started to record relatively long-period signals to ensure sensitivity to earthquakes from around the globe (so-called teleseismic waves) and to avoid the noise of microseisms: ocean wave energy that couples into the Earth's crust. The down-side to this focus was that in practice such a horizontal pendulum requires great care in setting up, and that the sensitive balance required for accurate operation is easily lost for the untrained. Nevertheless, this design remains popular among a large group of seismology enthusiasts worldwide.

Since the introduction of the Lehman horizontal pendulum, educators around the globe have explored alternative spring-based vertical seismographs. These often record preferentially shorter-period signals, but are simpler and more robust than the Lehman design (e.g. Braile *et al* 2003). This makes such sensors perfectly suited for the classroom environment. Other successful outreach and education efforts are centred on accelerometers housed in every-day electronics. These sensors are not optimally suited for earthquake signal recording, but rely on a 'strength in numbers' approach, where many signals—especially

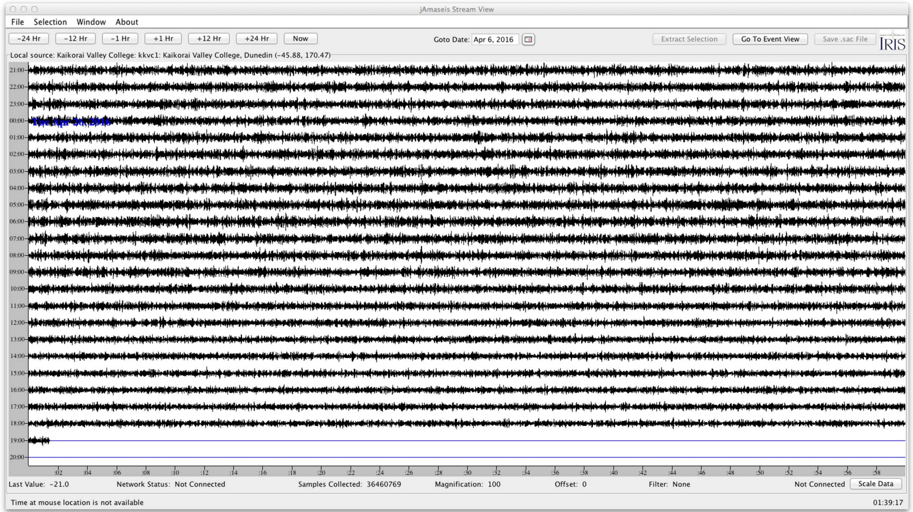

Figure 2. Seismic recording of a typical day at station KKVC1. Each horizontal line represents one hour of ground displacement at Kaikorai Valley College, Otago (New Zealand).

strong ones near the epicentre—are averaged to improve the quality of the sum (Cochran *et al* 2009).

Educational seismic networks operate successfully in the USA, the UK, France, Switzerland, and Australia. Recently, we have set up a network that exposes students in primary, secondary and tertiary education to seismic activity in and around New Zealand (figure 1). At the same time, our efforts highlight cultural indigenous heritage on this topic, captured by the Māori deity of earthquakes and volcanoes, Rūaumoko. The abbreviated version 'Rū' is the name of the New Zealand educational network of seismometers. Its ongoing results and discussions can be viewed at http://ru.auckland.ac.nz.

van Wijk *et al* (2013) describe the hardware of the Rū network: a vertical component sensor based on a Slinky toy and an Arduino Uno is literally transparent for the user to explore its functionality. Helicorder software *jAmaSeis* is freely provided by the Incorporated Research Institutions in Seismology (IRIS) at http://iris.edu/hq/jamaseis/. This software also facilitates the sharing of seismic data. At this moment, three of the Rū stations' data are directly available in *jAmaSeis*.

Next, we will highlight two applications of the recorded seismic data that help explore the internal structure of the Earth. We will first introduce a traditional earthquake location exercise. This exercise is available as a jupyter notebook (van Wijk 2016b), including a link to the seismic data used (van Wijk 2016a). Then, we will use Rū data to illustrate an application related to more recent developments in seismology: exploring (ocean) noise in seismic data as a signal to make inferences about the Earth's interior.

2. Applications

The stations in the Rū network of educational seismometers typically show signals such as the one depicted in figure 2. We call the recording of seismic waves a *seismogram*. Continuous

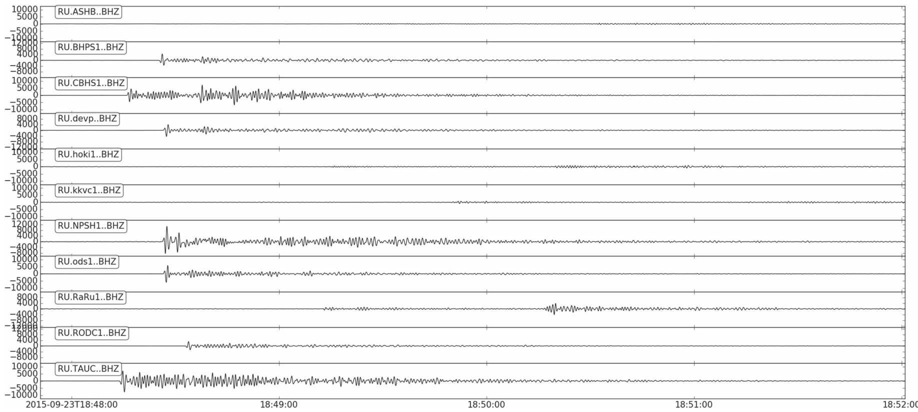

Figure 3. Seismic data representing ground vibrations at 11 stations in the Rū network. Time is on the horizontal axis, and the vertical scale represents ground displacement (in arbitrary units).

recordings of seismic data historically happened on long paper records spooled on rotating drums, a system dubbed a 'helicorder'. Typically, in seismograms recorded on helicorders time runs along the horizontal axis, and the vertical scale is a measure of ground displacement, velocity or acceleration at the station location. In this manuscript, we will represent the seismogram as $u(x, t)$, where u is the vertical displacement that is a function of time t and space[2] x.

Seismic signals are the result of small ground displacements with a seemingly random character, occasionally overprinted by the arrival of coherent seismic waves from earthquakes. However, the incoherent 'noisy' part of the signal can be caused by a host of sources that include the electronics in the hardware, but also from vibrations caused by human activity, winds shaking trees and buildings, and ocean waves crashing against the nearest shores. In the second example of this manuscript, we will exploit the noise caused by ocean waves crashing the shore.

Next, we take the reader through an analysis of seismic data recorded with our educational network. All data analysis is done in a Python-based (free) software suite titled 'Obspy' (Krischer *et al* 2015), but particularly the earthquake location exercise can be done with pen and paper, as well. Starting at the very basics of wave propagation, aimed at the level of secondary education, we will incrementally increase complexity to the analysis to retrieve more detailed information hidden in these seismic recordings. The final analysis of seismic data of ocean noise is an area of active research in the seismology community, but we hope the level of the discussion on the topic as presented here suits physics and geoscience undergraduate students of tertiary education.

2.1. Earthquake location

On 23 September 2015 (UTC), seismic quiescence was disturbed by the recording of an earthquake on the Rū network of seismometers. Stronger signals than the average background level in the seismograms of figure 3 represent ground motion caused by the arrival of seismic

[2] In general, seismic waves are measured in three orthogonal components, such as vertical, East–West, and North–South.

waves excited by an earthquake. These 4 minute long seismograms are sorted alphabetically on their school station names. The first-order observation is that for those stations where the seismic waves arrive earlier, the amplitude of these signals is generally larger. Intuitively, a later arrival of the seismic wave generally means that a particular station is farther from the earthquake. The amplitude of seismic waves decays with increasing distance from the earthquake for three reasons. First, seismic wave energy is transferred to other types of energy, predominantly heat. Second, seismic waves scatter—refract—at each impedance contrast faced in the Earth. Finally, the energy released by an earthquake is geometrically spread following conservation of energy. In the case of volumetric (body) waves, the seismic energy spreads in three dimensions. In addition, the amplitudes recorded in seismograms are affected by the coupling of the sensor to the ground, and local site effects.

We can use the amplitude and phase information of each seismogram for a qualitative approach to estimating the epicentre of this earthquake. The seismogram with the greater amplitude, or the earlier arrival time of the wave is recorded closer to the epicenter. An analysis of many stations will result in a region on the map containing the epicentre. The success of this qualitative method depends on a number of factors, most notably the distribution of the network stations, with respect to the epicentre.

Recordings of the fastest seismic wave at a seismic station are associated with the primary seismic wave, or *P*-wave, for which the particle motion is in-line with the direction of propagation; consisting of successive rarefactions and compressions. The *P*-wave travel time is the length of the path divided by the *P*-wave speed along this path. The wave speed—a function of the varying rock properties in the Earth—varies along its path. As a result, the *P*-wave travel time involves an integral along the path, with each infinitesimally small path section (dr) having its (local) wave speed $v_p(r)$. The *P*-wave arrival time t_p is the travel time from the origin time t_0:

$$t_p = t_0 + \int_P 1/v_P(r)\mathrm{d}r. \tag{1}$$

Note that the overall character of the seismograms $u(x, t)$ in figure 3 varies from station to station (i.e., varies as a function of distance 'x'). The most contrasting examples are the seismograms of stations TAUC and RaRu1: TAUC's signals are strong in amplitude early in time, and decay almost monotonically. RaRu1, on the other hand, has two distinct arrivals. The arrivals after the primary wave include secondary waves, or *S*-waves, which exhibit transverse polarisation and are by definition slower than primary waves. The *S*-wave arrival time is

$$t_s = t_0 + \int_S 1/v_S(r)\mathrm{d}r, \tag{2}$$

where v_S is the shear-wave velocity along the path from the earthquake to the seismograph. In general, we do not know the location of the hypocentre, nor the origin time of the earthquake. However, the origin time t_0 cancels in the expression for the *difference* between the *S*- and *P*-wave travel time:

$$t_S - t_P = \int_S 1/v_S(r)\mathrm{d}r - \int_P 1/v_P(r)\mathrm{d}r. \tag{3}$$

In general, the larger the arrival time difference between *P*- and *S*-waves on a particular station, the greater the distance between the station and the epicentre (epicentral distance). Because the velocity models of the Earth for primary and secondary waves $v_P(r)$ and $v_S(r)$ are relatively well established, we can quantify the estimate of the epicentral distance, based on the arrival time difference between *P*- and *S*-waves. For the purpose of a first-order epicentre

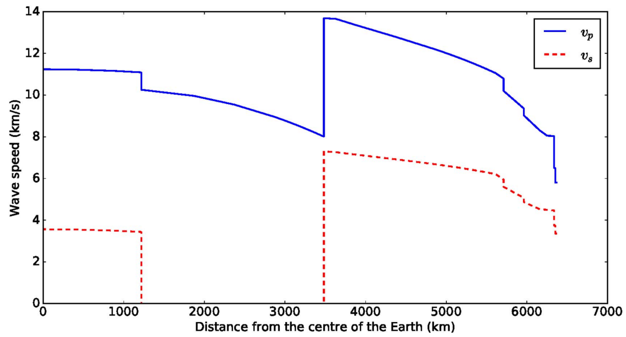

Figure 4. Seismic wave speed in the Earth, according to the IASP91 model.

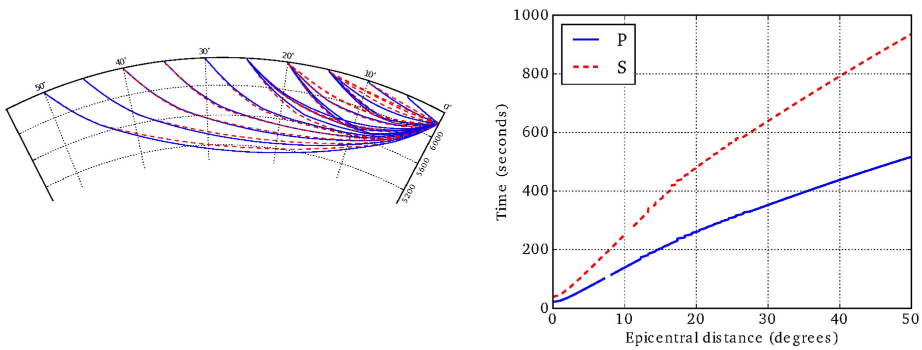

Figure 5. Ray paths (left) and travel times (right) as a function of epicentral distance for *P*- and *S*-waves in the IASP91 model. In this example, the earthquake occurred at a depth of 167 km.

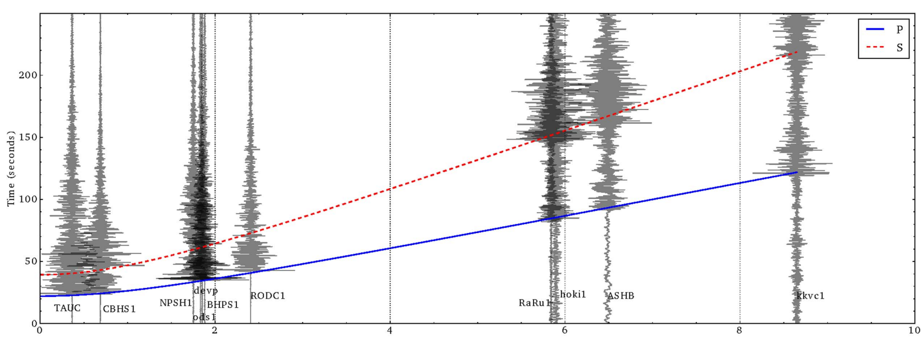

Figure 6. The same seismic data as in figure 3, but each seismogram is normalised to highlight the weaker waves at greater epicentral distance and greater travel times. The curved lines represent arrival times of the direct compressional (solid) and shear wave (dashed) for an EQ located near Roturoa, New Zealand, as predicted by the spherically symmetric seismic velocity model IASP91.

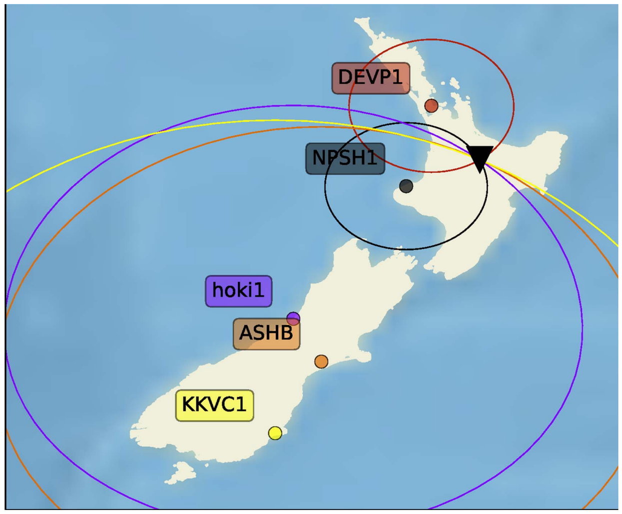

Figure 7. Each circle represents the estimated distance from station to the epicentre, based on the difference between *S*- and *P*-wave arrival time and the IASP91 seismic velocity model. These circles (almost) intersect near Rotorua, NZ. Map made with the free software Cartopy (Met Office 2010–2015). Made with Natural Earth. Free vector and raster map data @ www.naturalearthdata.com. Cartopy is published under the LGPLv3 licence.

estimate, the Earth's velocity model is spherically symmetric. The first such velocity models were based on the careful analysis of seismic waves from earthquakes recorded on stations around the globe by Jeffreys and Bullen (1958), whereas more recent seismic wave speed models use many more earthquakes and stations (e.g., the IASP91 model in figure 4, based on Kennett and Engdahl 1991).

For a given velocity model, such as the IASP91, both the ray path and the travel time for a given hypocentre can be calculated for any seismometer location via a technique called 'ray tracing'. An assumption of high-frequency waves allows us to reduce the wave equation to the Eikonal equation, resulting in efficient—but approximate—numerical solution to the path and travel time of a seismic wave. Figure 5 presents *P*- and *S*-wave ray paths (left) and travel times (right), as a function of epicentral distance, using the free software TauP (Crotwell *et al* 1999), which can be run stand-alone or from within the Obspy software. Note that as the seismic wave speeds vary, rays bend as prescribed by Snell's law (see the left panel of figure 5).

2.1.1. Example. Based on the IASP91 model, predicted arrival times for *P*- and *S*-waves are drawn in figure 6 for epicentral distances up to 10°. The *P*- and *S*-wave arrivals of a seismogram will uniquely 'fit' at the correct epicentral distance. For most seismograms in figure 3, the shear-wave arrival is not clear. Besides some limitations of our educational hardware, there are fundamental aspects to the difficulties of picking *S*-waves in a seismogram. For small epicentral distances, for example, the faster *P*-wave has not separated from the slower *S*-wave, yet. In this case, *P*- and *S*-waves have not separated on TAUC, but clearly have on RaRu1 (figure 3). Stations such as DEVP1 show the onset of this wave separation in time. For larger distances, where S- and *P*-waves have separated, diffracted *P*-

waves and other phases obscure the *S*-wave arrival. In addition, for larger epicentral distances, Snell's law for the velocity structure of the Earth shows the incidence angle of *P*- and *S*-waves to be (nearly) orthogonal to the surface (see the left panel of figure 5). In that case, shear-waves will be hard to detect on a seismogram representing the vertical component of ground displacement. As a result, we did not directly estimate the epicentral distance from our seismograms, but instead determined the epicentral distance from the coordinates of the seismographs to the epicentre estimated with the professional GeoNet network.

On 23 September 2015, at 18:47:51 (UTC) an earthquake of magnitude $M = 5.1$ occurred near Rotorua, NZ (38.32S, 176.14E), at an estimated depth of 161 km (http://geonet.org.nz/quakes/region/aucklandnorthland/2015p718332). The depth of the earthquake is estimated from the differential of the pP and the P phase. The pP phase is a wave that travels upward from the earthquake, reflects at the Earth's surface, and then propagates as a direct *P*-wave to the seismograph.

For each station, the time between the arrivals of the *S*- and *P*-wave results in an estimate of its distance to the earthquake. A circle centred on the station with a radius equal to this epicentral distance estimate can be drawn on a map. In principle, three stations are enough to estimate the epicentre. However, more stations (i.e., more circles) improve the accuracy of the epicentral estimate.

Placing normalised versions of the seismograms of figure 3 at their computed epicentral distance in figure 6, we observe a match between observed arrival times and those predicted for a spherically symmetric earth. Discrepancies between observed and predicted arrival times are on the order of a few percent. These small discrepancies are addressed in iterative updates to the local seismic velocity model in a process called 'seismic tomography', which plays an important role to reveal local variations in the Earth's structure. In turn, earthquake locations can be refined with these updated velocity models. The circles in figure 7 intersect at the black triangle; the epicentre reported by the national network installed and operated by GeoNet.

Finally, it should be noted that *jAmaSeis* provides an interactive tool to estimate the epicentre of an earthquake, based on the application of the principles discussed here, using seismograms from around the globe. There are also tools available to estimate the magnitude of the earthquake based on the arrival times and amplitudes of the recorded seismograms, but the amplitude response of the TC1 seismometers in our network is not currently calibrated for this task.

2.2. Seismic interferometry

Wave motion in our oceans couples into the Earth's crust in the form of seismic waves, which can be recorded on seismometers around the world. For the purpose of earthquake seismology, filters to remove the ocean-noise frequencies are implemented in the hardware, or applied in post-processing. Ocean-noise generated seismic waves can, however, be used to learn about the internal structure of the Earth. Seismologists now use seismic signals of ocean noise on seismic stations (and actually—in a case of complete role reversal—filter out the recordings of earthquakes). The analysis of days, or weeks, or sometimes even months of seismic noise results in estimates of the impulse response between seismic stations; as if a surface wave originated at one seismograph and is recorded at the other. In a heterogeneous medium such as the Earth, surface waves exhibit dispersive properties due to the velocity structure of the Earth. As an example of an inverse problem, recordings of such dispersive surface waves—caused by ocean noise—are used to infer subsurface structure in the Earth. We will retrieve estimates of the impulse response between seismic stations with data from our educational network of seismometers.

Figure 8. Ambient ocean noise impending from the left of station A at $x = 0$ with S_{L}, and from the right of station B at $x = L$ with S_{R}.

The principle of seismic interferometry is that seismic signal that passes from one station to the other can be retrieved via cross-correlation. The result is as if the first station is the location of a (virtual) seismic source, recorded at the other station. That ocean waves couple weakly into the solid earth in the form of surface waves has long been reported by Gutenberg (1911, 1921). Correlating long time series from two locations, we retrieve a virtual seismogram between these stations. This technique is particularly powerful in regions lacking actual earthquakes to probe the Earth's interior. Next, we will derive this result in a homogeneous medium with velocity c, in one dimension, closely following Snieder and van Wijk (2015).

Consider a seismogram $u(x, t)$, with a temporal Fourier transform:

$$u(x, t) = \frac{1}{2\pi}\int_{-\infty}^{\infty} U(x, \omega)\exp(-\mathrm{i}\omega t)\mathrm{d}\omega, \tag{4}$$

and a spatial Fourier transform:

$$u(x, t) = \frac{1}{2\pi}\int_{-\infty}^{\infty}\int_{-\infty}^{\infty} U(k, \omega)\exp(\mathrm{i}(kx - \omega t)\mathrm{d}\omega\mathrm{d}k, \tag{5}$$

where the wave number $k = \omega/c$. Now, the seismogram $u(x, t)$ is decomposed in plane waves represented by $\exp(\mathrm{i}(kx - \omega t)$ with coefficients $U(k, \omega)$. These plane waves travel in the x direction (right) for positive k, and in the $-x$ (left). In one-dimension, ocean noise sources can only come from the left ($s_{\mathrm{L}}(t)$) and the right ($s_{\mathrm{R}}(t)$) of the receiver, reducing the integral over all possible wave numbers to a sum:

$$U(x, \omega) = \int_{-\infty}^{\infty} U(k, \omega)\exp(-\mathrm{i}kx)\mathrm{d}k = S_{\mathrm{R}}(\omega)\exp(\mathrm{i}kx) + S_{\mathrm{L}}(\omega)\exp(-\mathrm{i}kx). \tag{6}$$

The expected value $\langle\cdot\rangle$ of the cross correlation of (random) ocean noise recorded at receiver A at $x = 0$ and B at $x = L$ as depicted in figure 8 is then:

$$\begin{aligned} C_{\mathrm{AB}}(\omega) &= \langle U(x = L, \omega)U^{*}(x = 0, \omega)\rangle. \\ &= \langle(S_{\mathrm{R}}(\omega)\exp(\mathrm{i}kL) + S_{\mathrm{L}}(\omega)\exp(-\mathrm{i}kL)(S_{\mathrm{R}}^{*}(\omega) + S_{\mathrm{L}}^{*}(\omega)\rangle \\ &= \langle|S_{\mathrm{R}}(\omega)|^2\rangle\exp(\mathrm{i}kL) + \langle|S_{\mathrm{L}}(\omega)|^2\rangle\exp(-\mathrm{i}kL), \end{aligned} \tag{7}$$

assuming the noise sources from the left and right are uncorrelated: $\langle S_{\mathrm{L}}(\omega)S_{\mathrm{R}}(\omega)\rangle = \langle S_{\mathrm{R}}(\omega)S_{\mathrm{L}}(\omega)\rangle = 0$. In the time domain, the cross-correlation is

$$C_{\mathrm{AB}}(t) = \frac{1}{2\pi}\int_{-\infty}^{\infty}[\langle|S_{\mathrm{R}}(\omega)|^2\rangle\exp(\mathrm{i}(kL - \omega t)) + \langle|S_{\mathrm{L}}(\omega)|^2\rangle\exp(-\mathrm{i}(kL + \omega t))]\mathrm{d}\omega. \tag{8}$$

Therefore, in the expected value of the cross-correlation of time series recorded at two stations, the term $\exp(\mathrm{i}(kL - \omega t))$ describes a wave that propagates from station A to B, while the term with $\exp(\mathrm{i}(kL + \omega t))$ describes a wave that propagates from B to A. This may be easiest to see in the case of impulsive noise sources, where these obey $\langle|S_{\mathrm{R}}(\omega)|^2\rangle = \langle|S_{\mathrm{L}}(\omega)|^2\rangle = 1$, for all values of ω. Then we can invoke the definition of the Dirac delta function (e.g., equation (14.31) in Snieder and van Wijk 2015) and find:

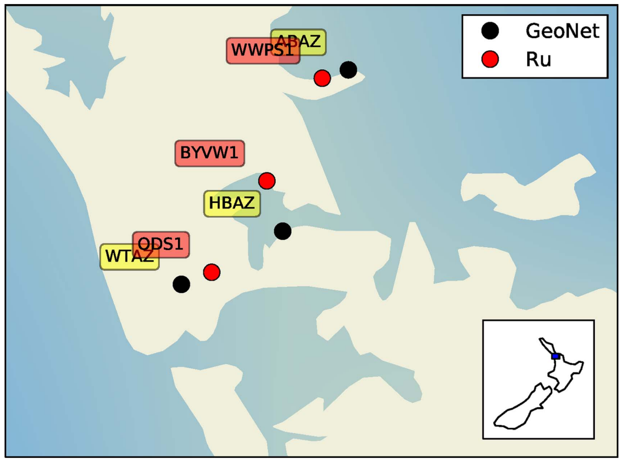

Figure 9. Rū and GeoNet stations used in the cross-correlation of ocean noise to retrieve the surface wave between the stations. The distance between ODS1 and BYVW1 is 17.5 km, and ODS1-WWPS1 is 36.8 km.

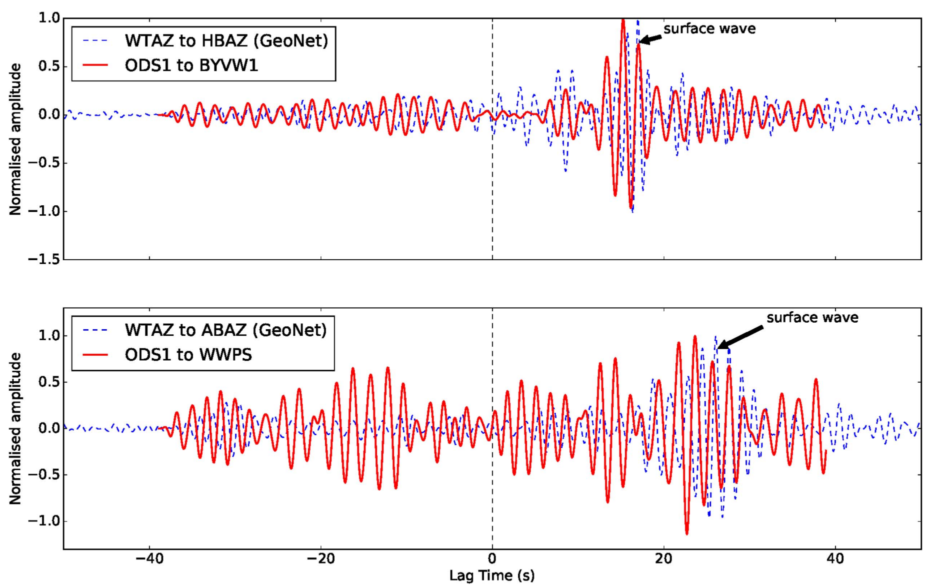

Figure 10. Normalised correlations of the time series from the west to the centre of the Auckland isthmus (top) and from the west to the east coast (bottom). Each panel contains the results for a pair of Rū stations compared to the closest GeoNet stations. Both networks show a surface wave travelling from West to East, represented by the maximum amplitude signals for positive correlation lags.

$$C_{AB}(t) = \frac{1}{2\pi}\int_{-\infty}^{\infty} [\exp(\mathrm{i}(kL - \omega t)) + \exp(-\mathrm{i}(kL + \omega t))]\mathrm{d}\omega. \\ = \delta(L/c - t) + \delta(L/c + t), \tag{9}$$

as impulses travelling a distance L with speed c from station A to B, and vice versa. The recovery of the impulse response between receivers can be generalised to arbitrarily heterogeneous media in two and three dimensions (Curtis *et al* 2006, Larose *et al* 2006, Snieder and Larose 2013).

2.2.1. Example. In the following example, A and B are two Rū school network stations, located between sources of ocean noise off New Zealand's west and east coasts that provide S_{L} and S_{R}, respectively (figure 9). The principles of seismic interferometry are illustrated by the cross correlation of 33 hours of recording at stations ODS1 and BYVW1 (17.5 km apart) and from ODS1 to WWPS1 (separated by 36.8 km).

Figure 10 contains the outcome of the correlation of the time series, defined by $C_{AB}(t)$ of equation (9). We compare the correlations $C_{AB}(t)$ for the Rū stations with the closest stations in the GeoNet network. The GeoNet data are filtered to match the frequency content of the TC1 seismometer used in the Rū network. Both panels present a distinct peak in the signal for positive lags (the right half). This peak is associated with a seismic surface wave that travels from Oratia Country Day School (west) via Bayview Primary School (top panel of figure 10) to Wentworth Private School (East, bottom panel). This wave is generated by ocean swells off Auckland's notoriously rough west coast. The generally calmer east coast does not generate such strong surface waves from east to west, confirmed by the lack of large-amplitude signal for negative lags in both panels of figure 10. In other words, $\langle|S_{\mathrm{L}}(\omega)|^2\rangle \gg \langle|S_{\mathrm{R}}(\omega)|^2\rangle$. The correlations of GeoNet station pairs match the Rū results in a qualitative sense, but the correlations for the shorter path length show a relatively stronger surface wave than the correlations for the longer distance pair. It will require the correlation of longer time series to increase the signal to noise ratio. The correlation functions also vary between the Rū and GeoNet stations, because the GeoNet stations are not in the exact same location as the Rū stations (figure 9).

Such surface wave recordings are used to infer subsurface information through a process called ambient noise tomography (ANT). In ANT, we estimate the surface wave speed as a function of frequency. Because the depth of penetration of surface waves is proportional to their wavelength, it is possible to estimate the seismic wave speed in the Earth as a function of space, and to infer subsurface geology from these velocity models. This idea has been successfully applied in the USA (Shapiro *et al* 2005), New Zealand (Lin *et al* 2007), and Europe (Yang *et al* 2007), for example. Unfortunately, our TC1 recordings are too narrow in terms of bandwidth to observe the dispersive behaviour of ocean-noise induced surface waves, but broader-band seismic surface wave information from ocean noise on GeoNet stations were analysed to infer subsurface structure of the Auckland Volcanic Field in Ensing (2016).

3. Conclusions

Developments in sensor hard- and software have improved data quality, and network capabilities for school seismology, making it easier for students of all levels to record and analyse their own seismic data, and share these with others. As a result, several national efforts in educational seismology thrive. We introduce some applications of educational seismology, ranging from the classic (earthquake location) to the more recently developed technique of seismic interferometry. While clear primary-wave arrivals with the vertical sensor used in our network are not always accompanied by outstanding secondary waves, an exercise based on the arrival time difference of these waves for stations in our network provides insights in earthquake location. (We provide the seismic data and the tools needed for the analysis consist of open-source software.) Similarly, recordings of ocean noise by our network are of such quality that the fundamental aspects of a new seismic imaging technique known as seismic interferometry and ambient noise tomography are clearly illustrated. Future work will focus on the development of more lessons with seismic data from educational seismic networks, and on efforts to improve robustness and accessibility of these data.

Acknowledgments

We thank support from the NZ Earthquake Commission (EQC Project 14/U690), the Foundation of the Society of Exploration Geophysics, and Science IT at the University of Auckland for the Rū project. We acknowledge the New Zealand GeoNet project and its sponsors EQC, GNS Science and LINZ, for providing GeoNet data to supplement the Rū data. In addition, we thank Ted and Linda Channel, Martin Smith and Chris Knudsen for their parts in developing the TC1 seismometer, Dr Daniel Hikuroa for all his efforts in making the Rū project a success, as well as all students and station managers of the Rū network.

References

Anderson J A and Wood H O 1925 Description and theory of the torsion seismometer *Bull. Seismol. Soc. Am.* **15** 1–14

Braile L W, Hall-Wallace M, Taber J and Aster R 2003 The IRIS education and outreach program *Seismol. Res. Lett.* **74** 503–10

Cochran E S, Lawrence J F, Christensen C and Jakka R S 2009 The quake-catcher network: citizen science expanding seismic horizons *Seismol. Res. Lett.* **80** 26–30

Crotwell H P, Owens T J and Ritsema J 1999 The TauP toolkit: flexible seismic travel-time and ray-path utilities *Seismol. Res. Lett.* **70** 154–60

Curtis A, Gerstoft P, Sato H, Snieder R and Wapenaar K 2006 Seismic interferometry-turning noise into signal *Leading Edge* **25** 1082–92

Ensing J 2016 Ambient seismic noise tomography in the auckland volcanic field *Master's Thesis* The University of Auckland

Gutenberg B 1911 Die seismische Bodenunruhe *PhD Thesis* Göttingen, Stürtz, Würzburg

Gutenberg B 1921 *Untersuchungen über die Bodenunruhe mit perioden von 4s–10s in Europa* (*Publications du Bureau Central de l'association Internationale de Sismologie*) (Strassburg: Bureau central de l'association internationale de sismologie)

Jeffreys S H and Bullen K E 1958 *Seismological Tables* (London: Office of the British Association)

Kennett B L N and Engdahl E R 1991 Traveltimes for global earthquake location and phase identification *Geophys. J. Int.* **105** 429–65

Krischer L, Megies T, Barsch R, Beyreuther M, Lecocq T, Caudron C and Wassermann J 2015 Obspy: a bridge for seismology into the scientific Python ecosystem *Comput. Sci. Discovery* **8** 014003

Larose E, Margerin L, Derode A, van Tiggelen B, Campillo M, Shapiro N, Paul A, Stehly L and Tanter M 2006 Correlation of random wavefields: an interdisciplinary review *Geophysics* **71** SI11–SI21

Lin F-C, Ritzwoller M H, Townend J, Bannister S and Savage M K 2007 Ambient noise Rayleigh wave tomography of New Zealand *Geophys. J. Int.* **170** 649–66

Met Office 2010–2015 *Cartopy: A Cartographic Python Library With a Matplotlib Interface* (Exeter: Met Office) (http://scitools.org.uk/cartopy)

Richter C F 1935 An instrumental earthquake magnitude scale *Bull. Seismol. Soc. Am.* **25** 1–32

Shapiro N M, Campillo M, Stehly L and Ritzwoller M H 2005 High-resolution surface-wave tomography from ambient seismic noise *Science* **307** 1615–8

Snieder R and Larose E 2013 Extracting Earth's elastic wave response from noise measurements *Ann. Rev. Earth Planet. Sci.* **41** 183–206

Snieder R K and van Wijk K 2015 *A Guided Tour of Mathematical Methods for the Physical Sciences* 3rd edition (Cambridge: Cambridge University Press)

van Wijk K 2016a Seismic data from Rūnetwork of the 2016 Rotorua earthquake 11 (https://figshare.com/articles/data_from_the_2016_Rotorua_earthquake_on_RU_stations/4246091)

van Wijk K 2016b Jupyter notebook to illustrate Earthquake location procedure 11 (https://figshare.com/articles/figures6and7EJP_ipynb/4248656)

van Wijk K, Channel T, Viskupic K and Smith M L 2013 Teaching geophysics with a vertical-component seismometer *Phys. Teach.* **51** 552–4

Walker J 1979 How to build a simple seismograph to record earthquake waves at home *Sci. Am.* **241** 152–61

Yang Y, Ritzwoller M H, Levshin A L and Shapiro N M 2007 Ambient noise Rayleigh wave tomography across Europe *Geophys. J. Int.* **168** 259–74